Experiment and modeling to evaluate the effects of proppant-pack diagenesis on fracture treatments

Dae Sung Lee [a,*], Derek Elsworth [b], Hideaki Yasuhara [c], Jim D. Weaver [d], Richard Rickman [d]

[a] Petroleum and Marine Research Department, Korea Institute of Geoscience and Mineral Resources, Daejeon, Republic of Korea
[b] Department of Energy and Mineral Engineering, Pennsylvania State University, University Park, PA, United States
[c] Department of Civil and Environmental Engineering, Ehime University, Matsuyama, Japan
[d] Halliburton Duncan Technology Center, Duncan, OK, United States

ARTICLE INFO

ABSTRACT

Observed reductions in the permeability of propped hydraulic fractures are examined by considering the role of mechanical stresses and the chemistry of pore fluids at elevated temperatures as agents of proppant diagenesis. Stress-enhanced dissolution of proppant increases the density of grain packing and reprecipitation of mineral matter further occludes pores — together these mechanisms additively reduce porosity and permeability. Experiments and analyses are presented which explore the evolution of porosity and permeability in proppant packs subjected to reservoir conditions of stresses to 65 MPa and temperatures to 177 °C. Experiments are completed in two modes: in flow-through reactors absent intergranular stresses to evaluate rates of dissolution and reprecipitation on proppant surfaces, and in uniaxially stressed reactors with stagnant fluids to evaluate the relative role of stress in mediating dissolution and porosity reduction. Lumped parameter models are used to evaluate rates of dissolution and chemical compaction in a range of proppants. Mechanisms include mineral dissolution, transport, and reprecipitation of the resulting products in the particle interstices, resulting in a loss of intergranular porosity. The model uses thermodynamic data derived from the reactor experiments to constrain the projected loss of permeability for the mineralogical composition of available proppants. Evaluated silica dissolution rates vary with temperature but are of the order of 1.1×10^{-11} to 3.1×10^{-4} mol/m^2 s in the range of 100 °C to 288 °C. Experimental results show chemical compactions of the order of 10 millistrains over 40 days and these project modeled reductions in porosity of the order of 25% over 1000 days. Rates of porosity loss increase both with an increase in temperature and a decrease in mean grain size of the granular proppant although ultimate porosities at the conclusion of compaction are similar. Rates and magnitudes of ultimate reductions in porosity map directly onto reductions in permeability and for proppants in the range 100 to 600 μm, result in permeability reductions in the range of 25% (163 °C) to 75% (191 °C). Such magnitudes (75%) of permeability loss over short periods (1000 days) are consistent with many field observations, with the mechanistic models providing a rational method of scaling such observations.

© 2010 Elsevier B.V. All rights reserved.

1. Introduction

Hydraulic fracturing is a common method of stimulating wells to efficiently recover hydrocarbons from low permeability reservoirs. As the hydraulic fracture is widened by the injection of fluids, sized particles (i.e., proppants) mixed with fracturing fluids are injected to hold fractures open. The ultimate goal of this treatment is to create a high-permeability and high-surface-area conduit that may access the fluids within the reservoir (Palish et al., 2007). These stimulations are expensive, and investors typically desire that the fracture treatment should remain a high-permeability conduit throughout the lifetime of the reservoir. However, recent evidence suggests that the performance of such treatments may be degraded early within the lifetime of production. These effects include multiphase, non-Darcy flow effects, gel damage, proppant pack damage by the fracturing fluid, proppant flowback, fines intrusion, proppant crushing, and proppant diagenesis (Weaver et al., 2005). Moreover, the internal or innate effects of the proppants utilized, such as types of proppants, proppant concentration, also control the fracture conductivity (Barree et al., 2003). These factors influence the overall effectiveness of the fracture treatment.

Fracture diagenesis, which is a physicochemical phenomenon, may exert a long-term influence on the fracture permeability among the identified external factors. In this work we address mainly this phenomenon that may be a dominant mechanism influencing a long-term change in the fracture permeability (i.e., the workability and

* Corresponding author.
E-mail address: leeds@kigam.re.kr (D.S. Lee).

Table 1
Flow-through experiments on synthetic proppants and reservoir rock mixtures.

Column	Sample	Experiments
1	Ohio sandstone	Fluid-pressure-only furnace experiments
2	20/40 Brady sand	
3	20/40 HSP 1	
4	20/40 HSP 1	
5	20/40 Brady sand	
6	Ohio sandstone + 20/40 Brady sand	
7	Ohio sandstone + HSP 1	
8	Ohio sandstone + 20/40 Brady sand	
9	Ohio sandstone + HSP 1	
1	20/40 HSP 2 + Ohio Sandstone	Ambient-stress quadcell experiments
2	20/40 ISP 2 + Ohio sandstone	

durability of wells). One of the main mechanisms of diagenetic compaction and deformation in sedimentary rocks is pressure solution[1] (e.g., Weyl, 1959; Rutter, 1976; Revil, 1999). Pressure solution, controlled by gradients of chemical potential differential between stressed-sites and free pore spaces, involves three linked processes of dissolution at the stressed interfaces of grain contacts, diffusive transport of dissolved mass from the interface to the pore space and finally reprecipitation at the less stressed, free-face of the grains (Yasuhara et al., 2003). This process results in temporally prolonged compaction and the concomitant reduction in bulk porosity and related permeability which has been shown to operate over engineering timescales (Yasuhara et al., 2003).

In this work we report flow-through experiments on synthetic proppants. We use a range of high strength proppants (HSP) through intermediate strength proppants (ISP) and sandwich these between coupons of reservoir rock mixtures (Table 1) to represent the walls of the fracture. These experiments are completed at temperatures in the range 121 to 177 °C and at confining stresses in the range 55 to 65 MPa. Experiments run over durations of up to 34 days to examine the intermediate-term evolution of permeability. These observations are fit to contemporary models of permeability reduction in granular aggregates where precipitation and pressure solution may influence mechanical and chemical compaction.

2. Proppant pack diagenesis by physiochemical compaction

Artificial proppants are complex mixtures of ceramic phases made by processing kaolin or bauxite at temperatures approaching 1450 °C. During this processing, proppants are engineered based upon the desired mechanical strength and durability to withstand ambient stresses, temperatures and chemical characteristics of the fluid, encountered in situ. When the formation is exposed to different pressure and temperature conditions, the rate of transformation is controlled by these pressure and temperature conditions. The chemistry-associated metastability of such engineered proppants is the key to understanding the related processes of pore compaction, grain-interpenetration, mineral redistribution, and extreme loss of permeability. Similar transformations and the rapid loss of permeability have been observed to participate in the diagenesis of reservoir rocks.

Proppants emplaced within hydraulic fractures are subject to an evolving stress field and to changes in chemical composition of the pore fluids. Immediately upon emplacement, the local in-fracture intergranular stresses will grow as the fracture treatment fluid

pressures diffuse into the wall-rock or back to the wellbore. These stresses will be of the order of the pre-stimulation minimum in situ stress. These bulk stresses are amplified at the grain–grain contacts of granular proppants elevating the potential for stress-corrosion cracking and the chemical potential (manifest as an increase in the reactivity or dissolution rate) at the contacts. Together, these effects have been shown to promote immediate mechanical compaction and to drive chemical compaction which may evolve over periods of years to millions of years. In this work we invoke such mechanisms of chemical compaction to describe the loss of function in-fracture treatments as chemical compaction proceeds and porosity and related permeability is degraded in the process.

One mechanistic model involves the action of elevated chemical potential at the grain–grain contacts which drive the compactive process. This process involves the action of three serial processes; dissolution at the grain–grain contacts, diffusion along the interfacial water film separating the grains, and precipitation on pore walls. This is illustrated in Fig. 1. First, dissolution at the contacts provides a source of mass into the pore via the interface, and is defined in terms of the dissolution mass flux, dM_{diss}/dt, the rate of addition of dissolved mass into solution at the interface, given by Yasuhara et al. (2003),

$$\frac{dM_{diss}}{dt} = \frac{3\pi V_m^2 (\sigma_a - \sigma_c) k_+ \rho_g d_c^2}{4RT},\tag{1}$$

where, V_m is molar volume of the solid, σ_a is the disjoining stress (e.g., Heidug, 1995) which is equal to the amount by which the pressure acting at grain-to-grain contacts exceeds the hydrostatic pore pressure, k_+ is the dissolution rate constant of the solid, ρ_g is the grain density, d_c is the diameter of the contacts, R is the gas constant, T is the temperature of the system, and σ_c is the critical stress, which defines stress state where the compaction of grain aggregate will effectively halt.

Secondly, based on Fick's first law, diffusion along the interface of the grain contacts is defined in terms of the diffusive mass flux, dM_{diff}/dt, as (Yasuhara et al., 2003),

$$\frac{dM_{diff}}{dt} = \frac{2\pi \omega D_b}{\ln(d_c/2\varepsilon)} \left(C_{int} - C_{pore} \right),\tag{2}$$

where, D_b is the diffusion coefficient, ε is infinitesimal length (1/1000, initial diameter of contact area), d_c is the diameter of the grain-to-grain contacts, and $(C_{int})_{x=\varepsilon}$ and $(C_{pore})_{x=d_c/2}$ are concentrations in the interface and pore space, respectively. ω is the thickness of the water film trapped at the interface.

Finally, precipitation of solute to the free faces of pore wall is defined in terms of the precipitation mass flux, dM_{prec}/dt, the rate of deposition of solute from the pore space onto the free-walls, is defined as (Yasuhara et al., 2006; Yasuhara and Elsworth, 2006; Elsworth and Yasuhara, 2006),

$$\frac{dM_{prec}}{dt} = k_- A_{pore} \rho_g V_m \left(\left(\frac{C_{pore}}{C_{eq}} \right)^m - 1 \right)^n,\tag{3}$$

where, A_{pore} is the nominal area of the void, k_- is the precipitation rate constant of the dissolved mineral, and C_{eq} is the equilibrium solubility of the dissolved mineral. m and n are two positive numbers normally constrained by experiment. In this work the constants are set to be unity because the dissolution kinetics of the proppants of interest are not be fully constrained and those of quartz, which may be considered a proxy of the proppants, have been identified to be unity (Rimstidt and Barnes, 1980).

At the applied stress and temperature condition, concentration of the material strongly influences compaction process, and the concurrent calculation to obtain the concentration is significant. Concentrations may be defined at the interface between grain

---

[1] We use the term pressure solution – in standard usage – to represent the process of stress-enhanced dissolution resulting from the elevated chemical potential of mineral at stressed contacts.
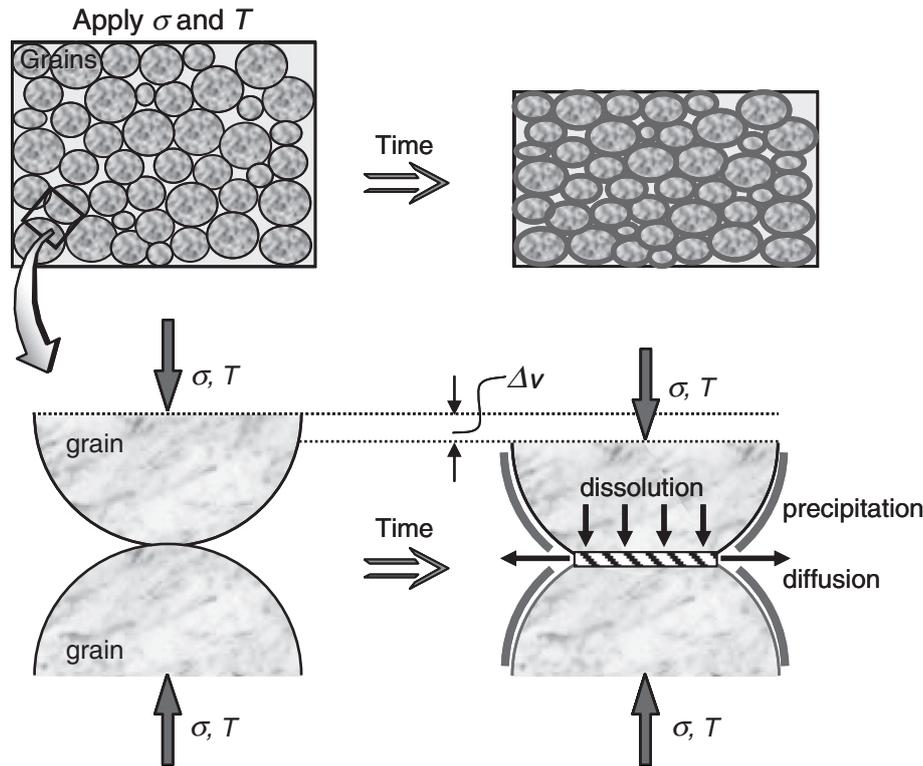
Fig. 1. Schematic of pressure solution for macroscopic aggregate and microscopic twin contacting grains. At the contacts the mineral dissolves due to high localized stresses and dissolved mass diffuses from the interface into the pore space. Finally, precipitation occurs at the free faces of the pore walls, resulting in the porosity (and related permeability) reduction.

contacts and pore fluid for both the closed and open system. For the closed system (e.g., Yasuhara et al., 2003),

$$
\left\{ \begin{array}{c} C_{int} \\ C_{pore} \end{array} \right\}_{t+\Delta t} = \left[\begin{array}{cc} D_1 + V_p/4\Delta t & -D_1 \\ -D_1 & D_1 + D_2 + V_p/2\Delta t \end{array} \right]^{-1}
$$

$$
\times \left[\left\{ \begin{array}{c} dM_{diss}/dt \\ D_2 \cdot C_{eq} \end{array} \right\}_{t+\Delta t} + \frac{1}{4\Delta t} \left[\begin{array}{cc} V_p & 0 \\ 0 & 2V_p \end{array} \right] \left\{ \begin{array}{c} C_{int} \\ C_{pore} \end{array} \right\}_t \right] \tag{4}
$$

where,

$$
D_1 = \frac{2\pi\omega D_b}{\ln}(d_c/2a), \quad D_2 = k\_A_{pore}\rho_g V_m C_{eq}, \tag{5}
$$

and Δt denotes the time step.

The three processes of dissolution, diffusion, and precipitation, coupled with the associated change in geometry, are combined to define the progress of porosity (and related permeability) with time. Evolution of permeability can be evaluated by the Kozeny–Carman equation (Bear, 1972) that relates the porosity to the permeability in porous media, as,

$$
k_r = \frac{k(t)}{k_i} = \frac{(1-\phi_i)^2}{(1-\phi(t))^2}\left(\frac{\phi(t)}{\phi_i}\right)^3, \tag{6}
$$

where k_r and k_i are the normalized and initial permeability, respectively, and ϕ_i is the initial porosity.

The main points of the overall calculation procedure are as follows. Initially, the system is treated as a closed system, with the representative repetitive structure comprising two hemispherical grains in contact, as illustrated in Fig. 2. Once stressed, during time step Δt, dissolution, diffusion, and precipitation mass are simultaneously calculated by Eqs. (1)–(3), respectively. Physically, the dissolved mass evaluated from Eq. (1) is supplied to the interface, and domain shortening proceeds as this mass passes along the

interface by diffusion. Some portion of the dissolved matter is removed from the interface as it exits into the pore fluid, as defined by Eq. (2). Depending upon the relative concentration differential between the pore fluid solution and the equilibrium concentration, a portion of the mass removed to the pore fluid is deposited to the grain surface (Eq. (3)) and the geometry of the grain is correspondingly modified. As a result, the porosity and related permeability of the system are evaluated and updated (Eq. (6)). Simultaneously, concentrations in the interface and pore fluid are updated utilizing Eqs. (4) and (5). To conduct a consistent calculation until the system reaches an equilibrium state, an iterative procedure is utilized.

3. Experiments

In order to understand the transformations that occur in the complex environment which evolves within a propped hydraulic fracture, a series of experiments were conducted that reproduced subsets of these hostile environmental conditions. The principal in situ characteristics are of elevated intergranular stress, high loadings of dissolved constituents within the pore fluids, and elevated temperatures, coupled with mechanisms of pore fluid flushing of the pore space. These characteristics were replicated in two series of experiments. The first suites of experiments were conducted at elevated temperatures with the flow-through of simulated reservoir fluids and at reservoir temperatures, but the compounding role of intergranular stress was absent. These enable the evolution of permeability to be directly measured and followed as a result of mineral dissolution, transport and reprecipitation — these are the furnace experiments. The second suite of experiments was conducted again at elevated temperatures but with stagnant fluids and no flow-through but with the important action of controlled and applied intergranular stresses. These enable the evolution compaction to be measured and the evolution of permeability to be inferred from the porosity, but including the important influence of the many stress-
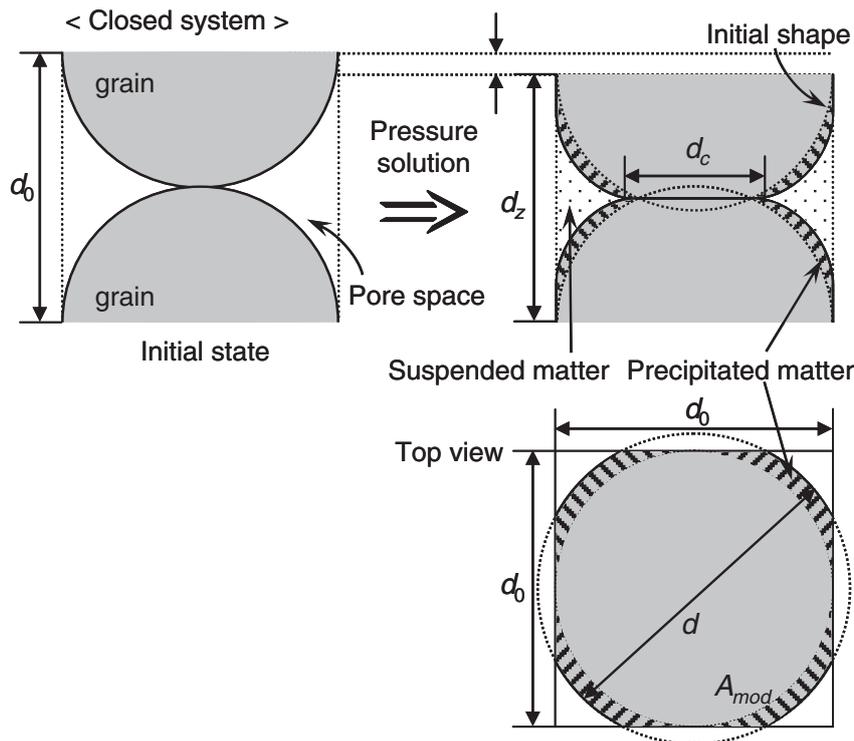
Fig. 2. Proposed geometric model of grain contact. Initially, two hemispheres of diameter, d_0, are in contact. As compaction proceeds ($d_z \leq d_0$), the diameter of the contact area, d_c, increases and the removed mass from the contact is suspended in the pore space and/or precipitated on the free faces. Grain geometries become truncated spheres of diameter, d, of cross-sectional area, A_{mod}.

related processes that are expected to be important in real reservoirs. These are the quadcell experiments, so-named since four experiments are completed on samples in parallel.

The results of such experiments where mineral-laden pore fluids and excess intergranular stresses are present resulting in the evolution of proppant-wall-rock indentation pits (Fig. 3a), infill structures within pores (Fig. 3b,c) and in the apparent crushing of grain–grain contacts (Fig. 3d,e,f) and the development of grain debris. The principles, principal mechanisms, methods of analysis and finally the results of these contrasting experiments are documented in the following.

The experiments are conducted to examine proppant compaction induced by high temperatures and pressures (i.e., proppant diagenesis). It should be understood that the experiments may overestimate rates and magnitudes of proppant diagenesis in situ, depending on magnitudes of field-scale dissolution and reaction rates. In the experiments, the compaction proceeds as interfacial water, which is a wetting agent, is present within interfacial grain contacts. Non-wetting agents of gaseous and liquid hydrocarbons, which are apparent in real reservoirs, may cause the compaction to be less active. The effects of the non-wetting materials exerted on the proppant diagenesis should be considered in future work.

3.1. Fluid-pressure-only furnace experiments

3.1.1. Experimental configuration

To examine the role of grain-surface dissolution and reprecipitation on the evolution of porosity and permeability within proppant packs, a series of flow-through experiments were conducted on bead-packs under anticipated in situ temperatures. Multiple flow-cells are charged with proppant and proppant-rock mixtures and upward circulation of simulated reservoir fluids induced by fluid circulation, as illustrated in Fig. 4. The cells are encased within a furnace and subjected to uniform temperatures to 177 °C. Flow rates are sufficiently slow that the fluid temperature equilibrates to the furnace temperature before reaching

the sample. Samples may be arranged in parallel in banks of five to examine flow through five individual proppant–rock combinations, or arranged in series to examine longitudinal flow along the flow path of an hydraulic fracture. The effluent fluids are collected at exit. Assays of mineral fluids both before and after flow-through enable a mass balance to be completed on circulation through the proppant pack. Measurements of fluid pressure drop across the sample to measure permeability change, and therefore corroborate permeability predictions are made at the conclusion of individual experiments.

3.1.2. Experimental observations

Experiments are conducted in the previously prescribed configuration at temperatures of 121 to 177 °C and for mixtures of HSP 1, sandstone formation material and Brady sand. Experiments are run at steady flow conditions and temperatures until steady outlet concentrations of dissolved components result. Net concentrations of silica are used to define rates of dissolution from equilibrium data, where silica rather than alumina is the controlling phase. The evolution of equilibrium silica concentrations are shown with flow rate for various experiments in Fig. 5. Notably, concentrations generally decrease with an increase in flow rate, implying a dissolution rate control on the evolution of the proppant pack, and enabling these data to be used to recover dissolution rates for the composite silica-alumina mineral surfaces.

3.1.3. Analysis

Since dissolved concentration generally decreases with an increase in through-flow rate, the dissolution process is dissolution rate controlled, enabling rate data to be recovered from the experiments. For a first-order reaction where the system is at a dynamic steady state, the mass removal rate of a mineral component dissolved in the circulating fluid, $\dot{M}$, may be equated with the dissolution rate as

$$\dot{M} = V_p \frac{A}{M} k_+ \left(c_p - c_{eq} \right) \tag{7}$$
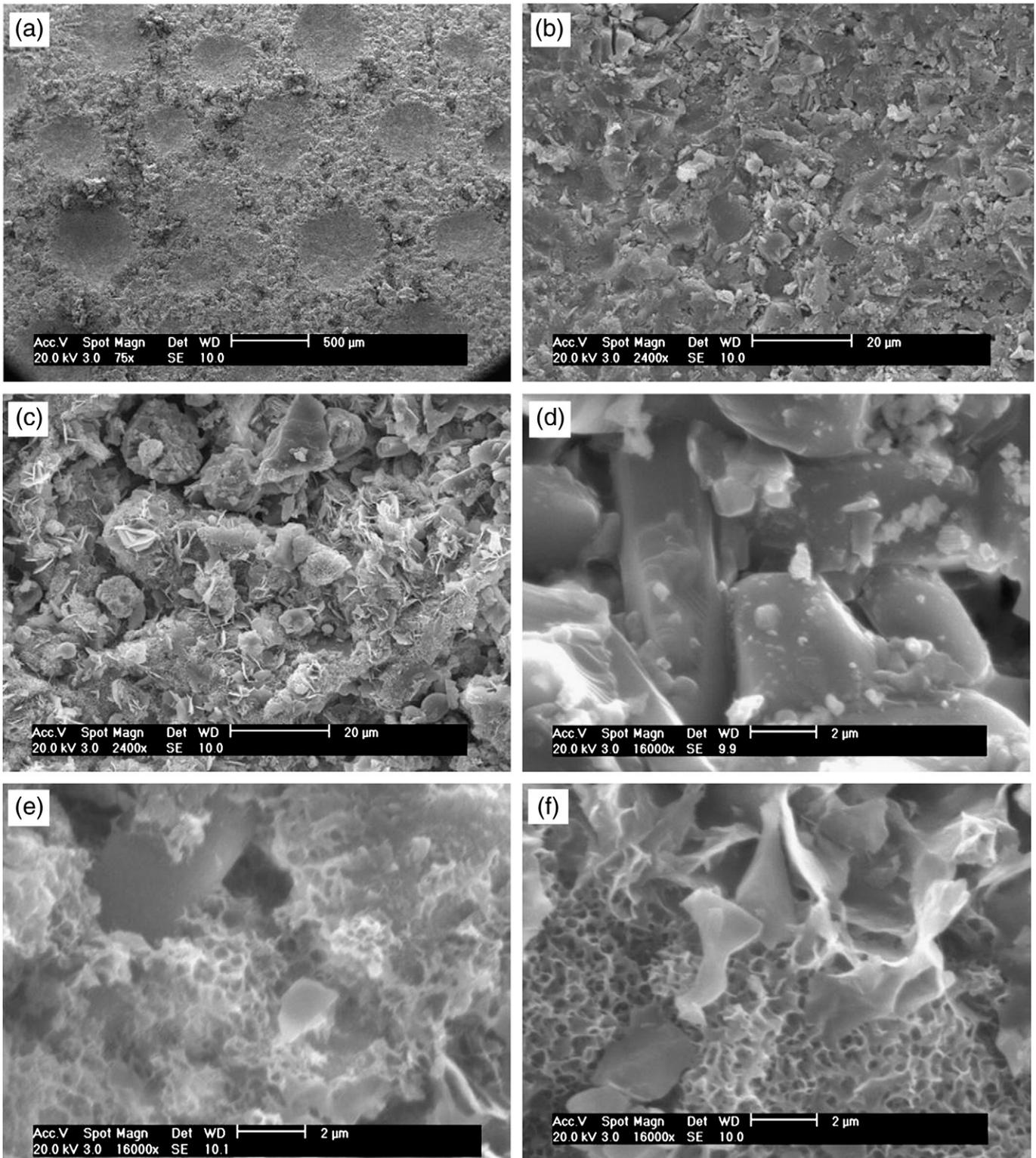
Fig. 3. Scanning electron micrographs of Brady sandstone wafers recovered from quadcell stress tests where the sandstone coupon is in direct contact with proppant. Bar lengths are 200 μm (a) 20 μm (b,c) and 2 μm (d,e,f). Note that the indentation pits of the proppant (a) are apparent at the lowest magnification and at successive magnifications the presence of (b,c) precipitates are apparent, together with (d,e,f) mechanical breakage of proppant and sand particles.

where A is the relative grain surface area, M is the mass of the fluid, V_p is the volume of the pores, k_+ is the dissolution or precipitation rate constant driven by the sense of the difference between concentration of the species in the pore fluid C_p relative to the equilibrium concentration C_{eq} where neither precipitation nor dissolution progresses. The mass flow rate of any component may be related to the pore volume, V_p, and the residence time of the fluid at concentration C_p within the sample, t_c as

$$\dot{M} = -c_p \frac{v_p}{t_c} = -c_p q \qquad (8)$$
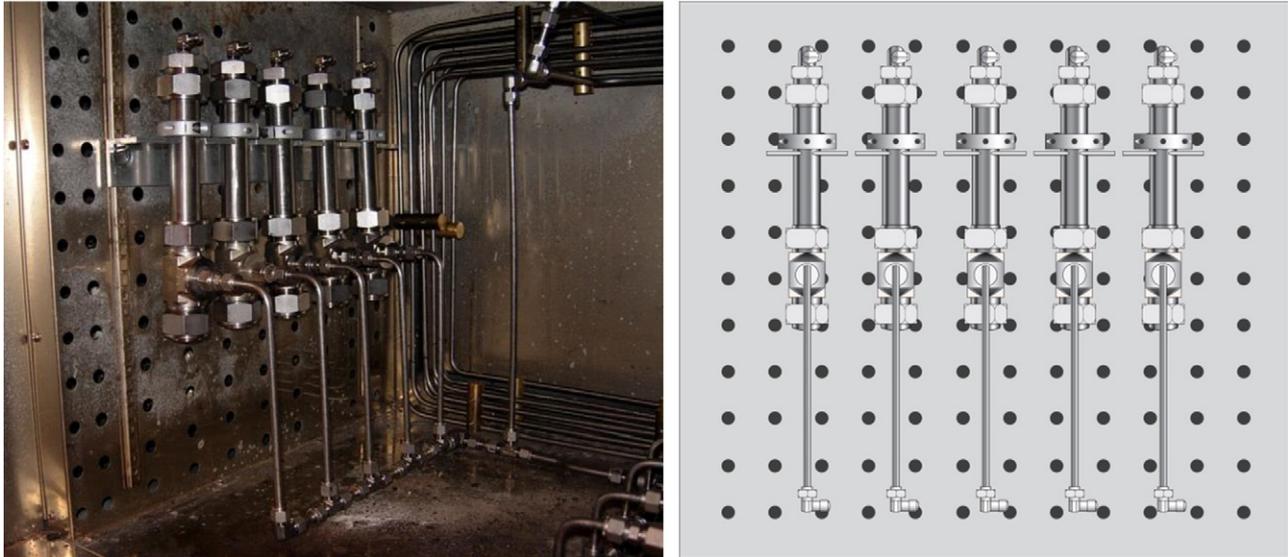
Fig. 4. Proppant-pack circulation cells for diagenetic studies. Proppant and host reservoir materials are placed in the circulation cell (vertical) and reservoir fluids circulated at elevated ambient temperature in the furnace. Fluid plumbing can be arranged to supply the same fluid into each cell (upwards from base) or to have output from one cell as the input to the base of the next for longitudinal studies. Solid stresses are uncontrolled but fluid pressures and flow rates are prescribed.
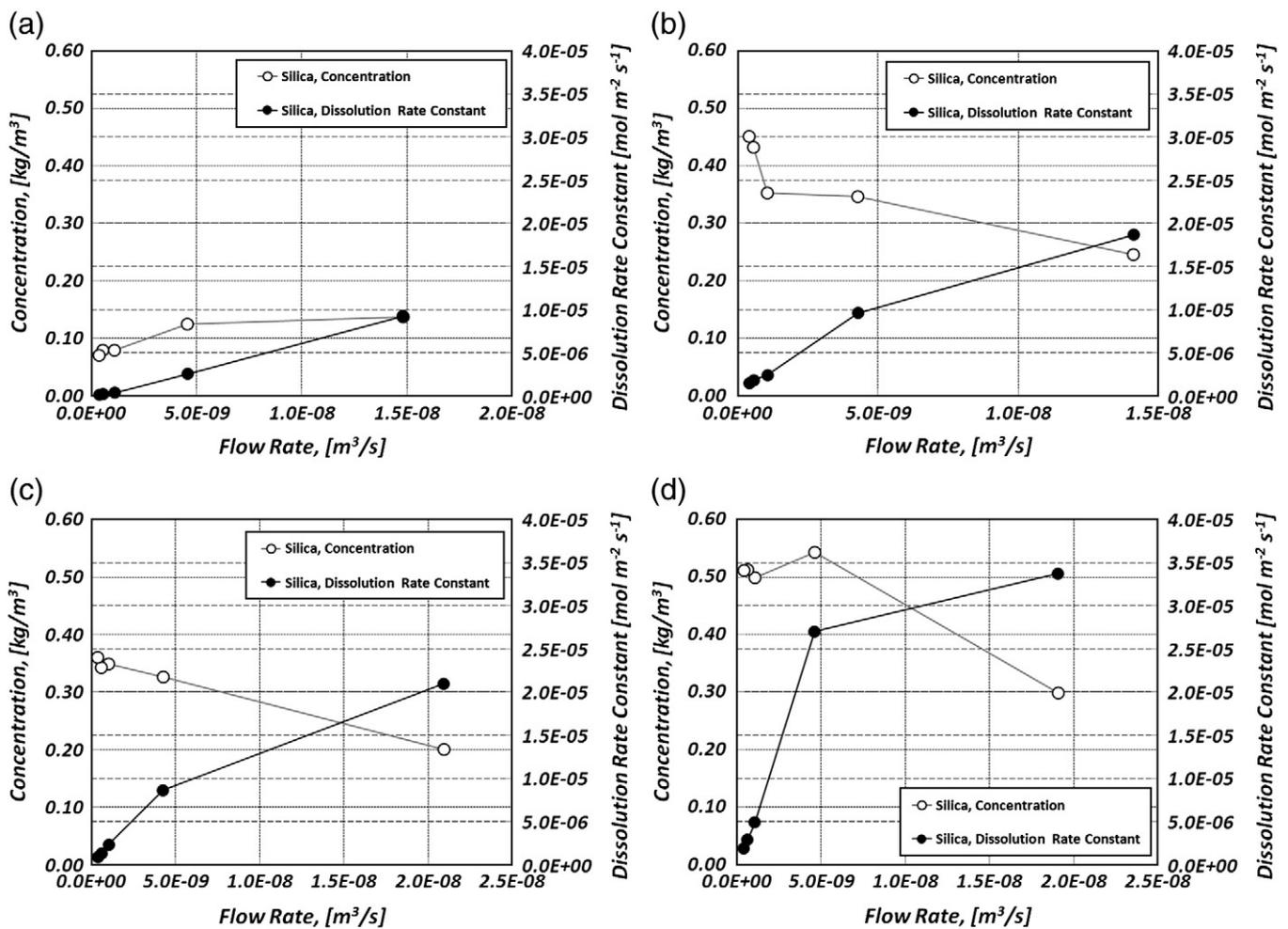
Fig. 5. Results of furnace tests for fluid circulation with (a) 20/40 HSP 1, (b) formation material ± 20/40 Brady sand, (c) 20/40 Brady sand, and (d) formation material ± 20/40 HSP 1. Changes in silica concentration with time and calculated dissolution rate constant from data.

Table 2
Silica dissolution rate constant recovered from the furnace cells at 289 °C.

Column	Sample	Silica, dissolution rate constant $(\mathrm{mol\ m^{-2}\ s^{-1}})$
6	Ohio sandstone + 20/40 Brady sand	6.82×10^{-6}
7	Ohio sandstone + HSP 1	6.83×10^{-6}
8	Ohio sandstone + 20/40 Brady sand	7.12×10^{-6}
9	Ohio sandstone + HSP 1	6.01×10^{-6}

Table 3
Chemical composition of the proppants used in these analyses (weight %).

Proppant	Al_2O_3	SiO_2	TiO_2	Fe_2O_3	Other
ISP 1	48	48	2	1	1
ISP 2	51	45	2	1	1
ISP 3	72	13	4	10	1
HSP 2	83	5	3.5	7	1.5

enabling mass flow rate to be equated with the fluid volumetric flow rate, q. This enables Eqs. (7) and (8) to be equated and therefore the magnitude of dissolution rate constant to be determined from

$$\frac{A}{M}k_+ = \pm \frac{c_p}{\left(c_p - c_{eq}\right)}\frac{q}{v_p} \qquad (9)$$

where all terms on the right-hand-side of Eq. (9) are determined from the experiment or from material data. These allow dissolution or precipitation rate constants to be determined from the laboratory data.

3.1.4. Results

Assuming steady-state dissolution, and no influence of pressure solution (no intergranular stress is applied), dissolution rate constants may be recovered from the effluent concentrations using Eq. (9). For flow rates in the range 0.0–2×10^{-8} m³/s the effluent concentrations generally decrease with increase in flow rate for aggregate mixtures of formation material, HSP 1, and Brady sand (Fig. 5b,c,d) but the unmixed HSP 1 (Fig. 5a) shows the opposite trend. Dissolution rate constants evaluated from these data are in the range 10^{-6} to 4×10^{-5} mol/m² s as illustrated in Fig. 5. These rate constants are consistent to within an order of magnitude for a variety of ceramic and silica proppants (Table 2).

3.2. Ambient-stress quadcell experiments

3.2.1. Experimental configuration

To examine the role of stress in mediating mechanical and chemical compaction of proppants present within a fracture, a series of experiments were conducted within a quadcell apparatus, as illustrated in Fig. 6. In this configuration a fluid-saturated proppant bead-pack is uniaxially compressed under applied stress. Deformation is measured with time for the compacting pack. The initial deformation is due to mechanical compaction and is complete within hours to a day. The subsequent compaction resembles creep compaction and diminishes in rate with time, and is a manifestation of the processes of chemical compaction noted in Section 2.

3.2.2. Experimental observations

Experiments have been conducted using different synthesized proppants (Table 3) at temperatures in the range 121 °C to 177 °C and at confining stresses from 55 MPa to 65 MPa to examine the evolution of compaction and related porosity evolution. These experiments result in chemical compactive strains in the range 0 to 8 millistrains which in turn may be correlated with the influences of pressure solution to determine mineral dissolution rates, in this case mediated by stress-enhanced chemical potential.

3.2.3. Analysis

The evolution of strain with time may be predicted form Eq. (7), allowing magnitudes of dissolution rate constant to be recovered from the compaction data. The dissolution rate constants for silica and aluminum are measured for different temperatures from the quadcell experiments and back calculated for a high temperature ($>$177 °C) as 3.10×10^{-4} mol/m² s¹ at 288 °C (Fig. 7). Especially for silica at high temperature, the quadcell-recovered rate constants are of similar order to those measured in the furnace tests (without pressure solution effects), 2.40×10^{-6}–$1.41 \times 10^{-}$ mol m^{-2} s^{-1} at 289 °C. The rate constants back calculated from the silica concentration data at different temperatures are related as $k_+ = 4 \times 10^{-6}e^{0.096(T)}$. These are higher than those reported in the literature and higher than measurements from the furnace data. However, this observation is

Fig. 6. Quadcell experimental arrangement showing four-part compression cell to apply constant stress to the top of a cylindrical sample of proppant sandwiched between wafers of host rock stagnant flow conditions.
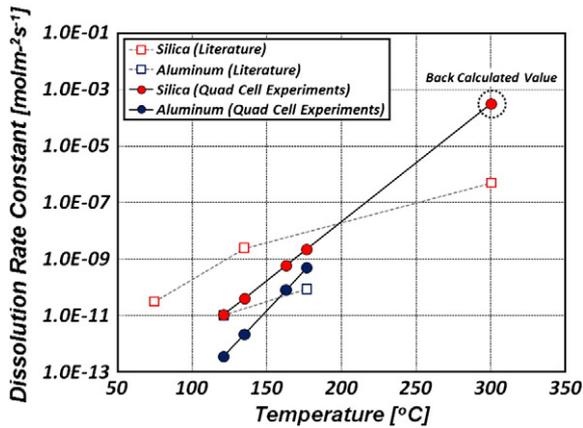
Fig. 7. Dissolution rate constants recovered from quadcell tests under 65.5 MPa and at temperatures of 121 to 177 °C (filled symbols) and compared with data from the literature (open symbols).

consistent with mechanical fracturing and the development of new surface area under stressed conditions (quadcell tests).

3.2.4. Results

The observed mechanical compaction data may also be fit directly to the modeled compaction data, implied by Eq. (4). This procedure is the same as using the dissolution rate data back calculated from the compaction data. Applying these rate coefficients enables the forward evaluation of compaction rate that will match the experimental data, but also allows extrapolation for future compaction history. Similarly,

from knowledge of the projected compaction history, the evolution of porosity and permeability may also be recovered.

This exercise is completed for the experiments on ISP 2 previously discussed and reported in Fig. 8. The fit between experimental and modeled data is shown in Fig. 8a where dissolution rate data are used from the aggregate range of experiments. Where these data are extrapolated in time, Fig. 8b shows that the compaction of 8 milli-strains measured after 40 days will evolve to more than 60 milli-strains after 1000 days. For a mono-dispersed granular aggregate of mean diameter of 600 μm, this corresponds to a reduction in porosity of about 3% over this period (Fig. 8c), and a corresponding reduction in permeability of the order of one-third (Fig. 8d). Where the aggregate is compacted at lower temperatures, the compaction rate is significantly reduced although ultimate compaction magnitudes will be comparable, as suggested in mechanistic models of this process (e.g., Yasuhara et al., 2003). Consequently ultimate changes in porosity and permeability will be similar as for the higher temperature case although the evolution will be slower.

4. Evolution of porosity and permeability in proppant packs

The rate data gathered from both furnace and quadcell experiments are used in the procedure described previously to identify trends in the evolution of porosity and permeability at reservoir conditions. The response of ISP 1 subject to a mean stress of 65 MPa is examined using these data by modeling response at 135 to 177 °C as illustrated in Fig. 9a. As noted previously, the porosity reduces most rapidly with an increase in temperature. With temperatures to 191 °C, the porosity after 1000 days is reduced by about a third from 0.35 to 0.25. As proppant size is reduced from 600 μm, to 100 μm (Fig. 9c), the rate of porosity
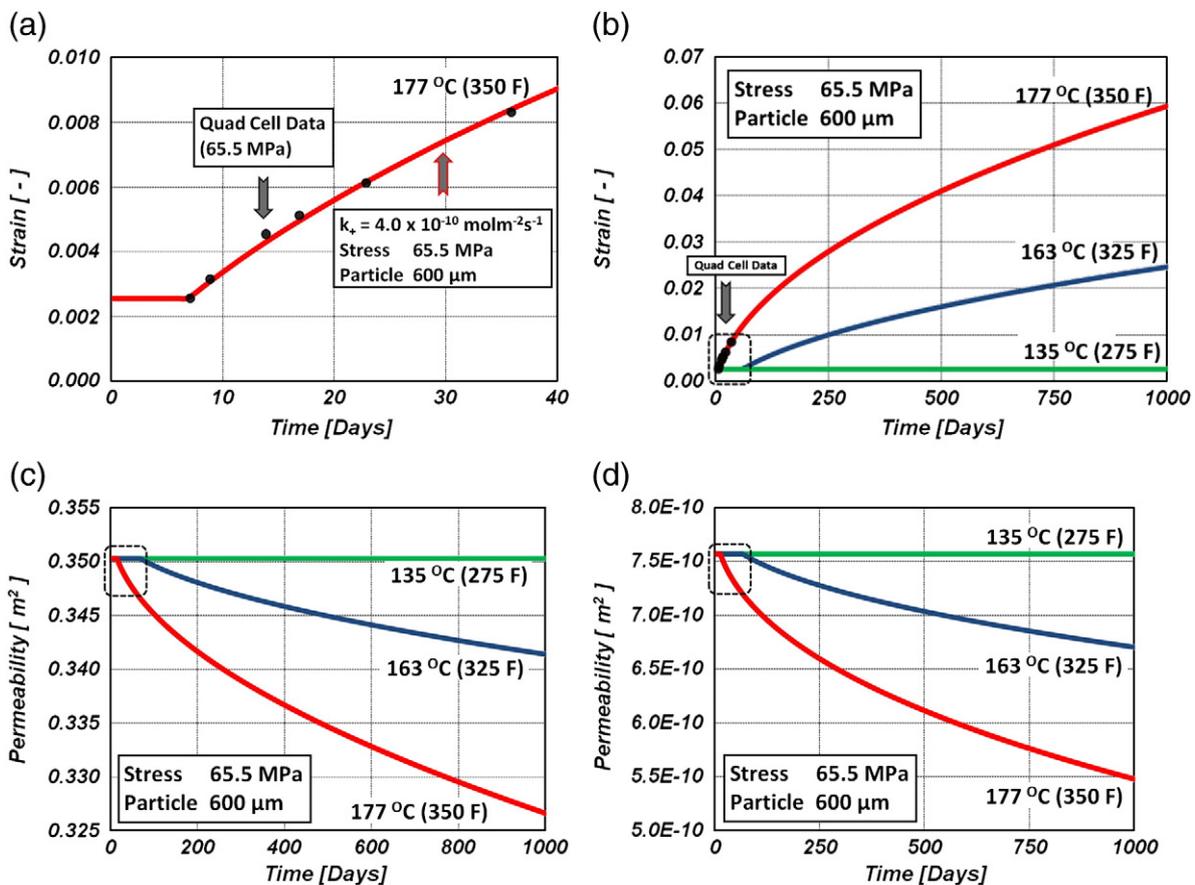
Fig. 8. Quadcell data for compactive strains in 600 μm diameter ISP 2 — Al$_2$O$_3$ (51 wt.%) and SiO$_2$ (45 wt.%) with time at 177 °C. Data are extrapolated through modelling-derived material coefficients to give (b) compaction over the first 1000 days. These results may then be used to predict the anticipated evolution of (c) porosity and (d) permeability for temperatures in the range 135 to 177 °C.
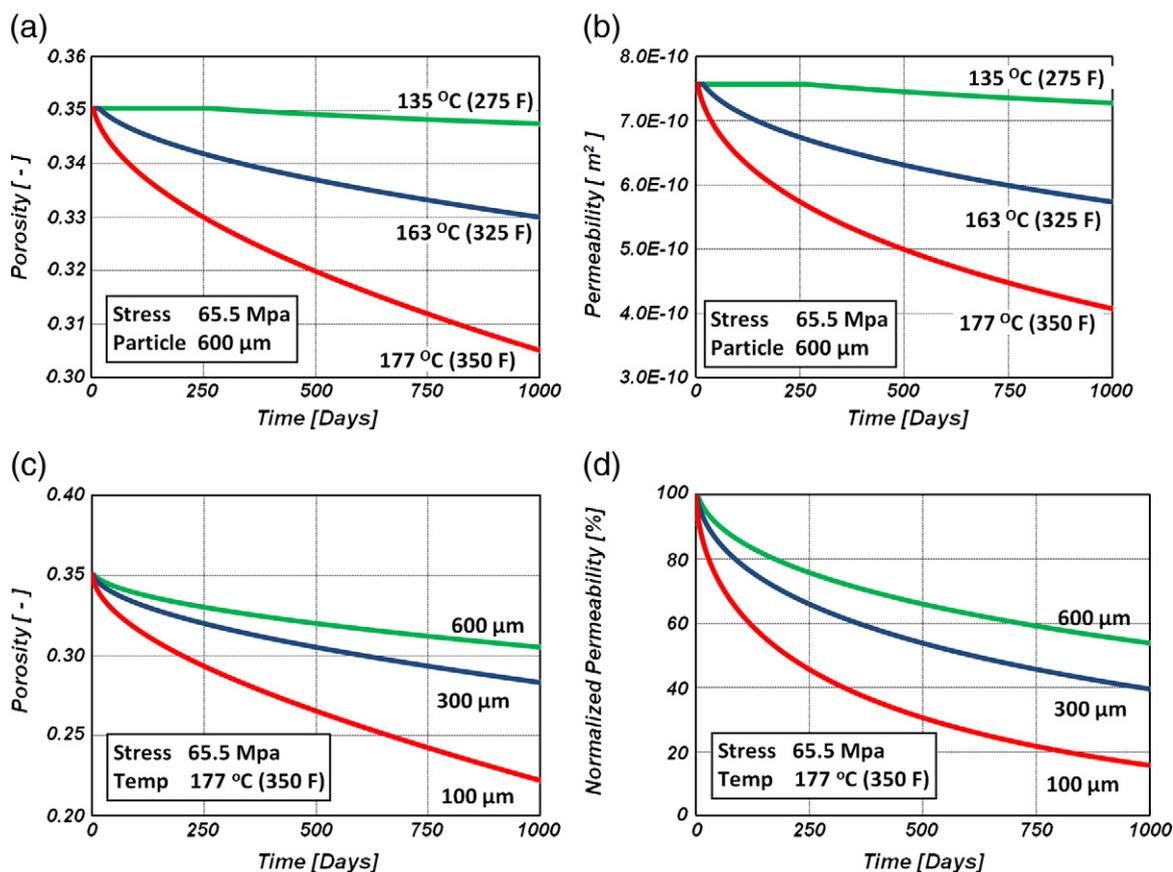
Fig. 9. Modeled evolution of (a) porosity and (b) permeability with temperatures in the range 135 to 177 °C for ISP 1 — at a diameter of 600 μm and comprising Al_2O_3 (at 48 wt.%) and SiO_2 (at 48 wt.%). Greatest changes are at highest temperatures. Reductions of (a) porosity and (b) permeability are greatest and most rapid as proppant grain size is decreased from 600 to 100 μm.

decline is further increased, resulting in an ultimate porosity of close to 0.2. Similarly, permeability magnitudes decrease most rapidly as temperature is increased, as illustrated in Fig. 9b, reducing by 75% for the case of 600 μm diameter proppant. Where the grain size is further reduced, normalized permeability reduces more rapidly reaching 15% of the initial permeability at 1000 days (Fig. 9d) for material of 100 μm diameter.

A similar procedure may be applied to predict the evolution of permeability data from the dissolution rate data recovered from experiments on other proppants. These proppants include HSP 2, ISP 1, and ISP 2. The recovered rate data from furnace and quadcell experiments are used, and assuming that compaction and pore occlusion is controlled by the remobilization of silica, rather than the much slower reaction rate for alumina, predicted changes in permeability with time are as shown in Fig. 10. Trends are similar to those noted before. For mono-dispersed gradations of 600 μm, permeability reduces most rapidly with increasing temperature, where all other factors are equivalent. In each of the three proppants in Fig. 10 the projected permeability reduces by about 75% over 1000 days but is slightly less for ISP 2. This lower reduction in permeability for ISP 2 is surprising as the rates of compaction should scale proportionately to the SiO_2 content, and HSP2 has a significantly lower proportion present. However, in this particular case, the results for HSP 2 are conditioned on mechanical data from the quadcell deformation experiments, and are likely more robust in exercising important mechanical mechanisms than the furnace data.

5. Conclusions

This work has evaluated changes in the porosity and permeability of proppants subject to stresses, chemistry, and temperatures consistent with hydrocarbon reservoirs of intermediate depth. Laboratory experi-

ments separately exercising roles of dissolution and precipitation, and of stress-mediated compaction have been evaluated in separate experimental configurations. The controlling material characteristics are the mineral dissolution rates of components present in the granular aggregates. The principal components are silica and alumina, with silica dissolution providing the rate limiting step.

A model for stress-enhanced dissolution at granular contacts has been used to interpret observations showing continuing compaction of proppant packs under constant temperature and stress. These observations are consistent with the removal of material from stressed contacts by dissolution, and its redeposition elsewhere within the pack, depending on whether the system is either open or closed to flow. Observations are used to inform a model to represent these behaviors.

In this work, the permeability of proppant packs have shown permeability declines of a few percent occurring in periods of the order of tens of days. Both the magnitude of the permeability loss, and its rate are observed to be exacerbated by elevated temperature (>135 °C), stresses (>55 MPa), and also by the chemical compositions of introduced fluids and proppants. Proppants with smaller grain sizes also compact more quickly. Extrapolations of ultimate permeabilities approach the order of 75% (191 °C) to 25% (163 °C) at the completion of dissolution-mediated compaction, and durations are accelerated as the temperature is increased. These effects are greater at higher temperatures.

Although constrained with important but meager data, these trends are anticipated to be relatively robust. These methods will also be applicable in indexing the performance of other proppants where rate data are available. Mechanisms for fracture diagenesis suggested by these experiments and their representation have suggested remedial strategies to reduce the impact of fracture diagenesis on well productivity, and to retain fracture permeabilities at post-completion levels.
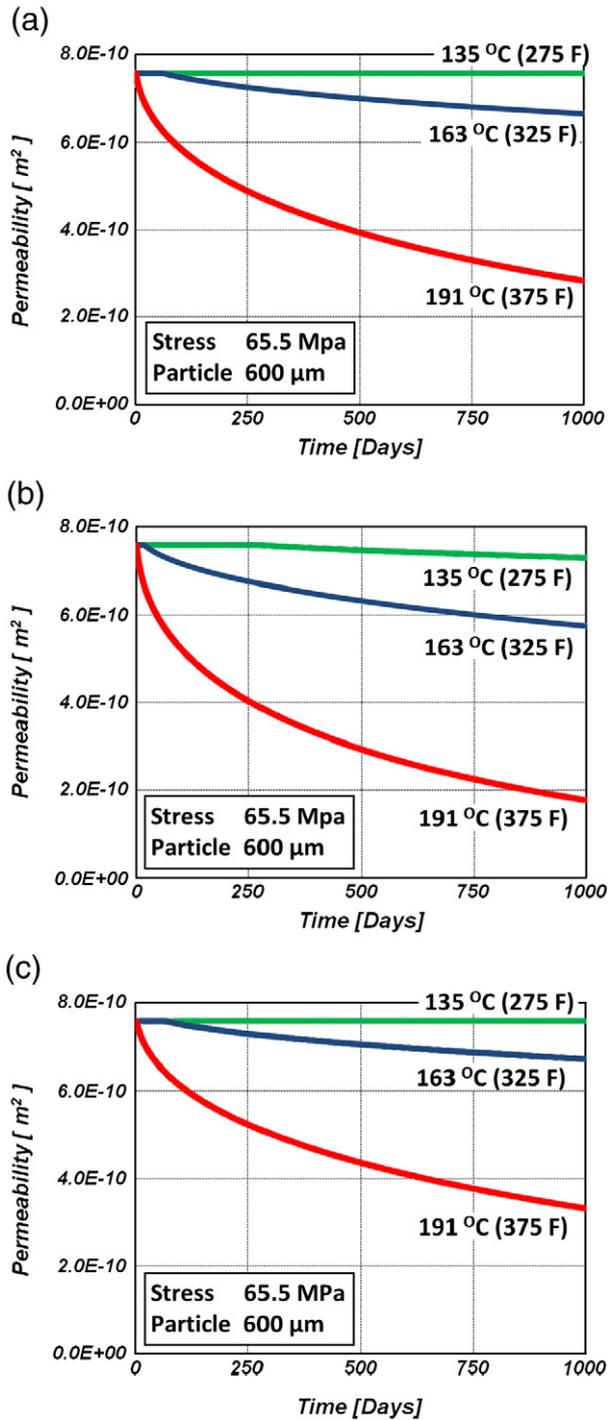
Fig. 10. Projected evolution of permeability in proppant packs at 65.5 MPa and 600 μm diameter for (a) HSP 2 [Al_2O_3 — 83 wt.% and SiO_2 — 5 wt.%], (b) ISP 1 [Al_2O_3 — 48 wt.% and SiO_2 — 48 wt.%], and (c) ISP 2 [Al_2O_3 — 51 wt.% and SiO_2 — 45 wt.%].

References

Barree, R.D., Cox, S.A., Barree, V.L., Conway, M.W., 2003. Realistic Assessment of Proppant Pack Conductivity for Material Selection. Society of Petroleum Engineers, SPE, p. 84306.

Bear, J., 1972. Dynamics of Fluids in Porous Media. Dover, Mineola, N.Y, pp. 162–165.

Heidug, W.K., 1995. Intergranular solid-fluid phase transformations under stress: the effect of surface forces. J. Geophys. Res. 100, 5,931–5,940.

Palish, T., Duenckel, R., Bazan, L., Heidt, H., Turk, G., 2007. Determining Realistic Fracture Conductivity and Understanding its Impact on Well Performance — Theory and Field Examples. Society of Petroleum Engineers, SPE, p. 106301.

Revil, A., 1999. Pervasive pressure-solution transfer: a poro-visco-plastic model. Geophys. Res. Let. 26, 255–258.

Rimstidt, J.D., Barnes, H.L., 1980. The kinetics of silica–water reactions. Geochim. Cosmochim. Acta 44, 1,683–1,699.

Rutter, E.H., 1976. The kinetics of rock deformation by pressure solution. Philos. Trans. R. Soc. London Ser. A 283, 203–219.

Yasuhara, H., Elsworth, D., Polak, A., 2003. A mechanistic model for compaction of granular aggregates moderated by pressure solution. J. Geophys. Res. 108 (B11) ECV 1~13.

Yasuhara, H., Elsworth, D., 2006. A numerical model simulating reactive transport and evolution of fracture permeability. Int. J. Num. Anal. Meth. Geomechs. 30 (10), 1,039–1,062.

Elsworth, D., Yasuhara, H., 2006. Short timescale chemo-mechanical effects and their influence on the transport properties of fractured rock. Pure Appl. Geophys. 163, 2,051–2,070. doi:10.1007/s00024-006-0113-3.

Yasuhara, H., Polak, A., Mitani, Y., Grader, A., Halleck, P., Elsworth, D., 2006. Evolution of fracture permeability through fluid–rock reaction under hydrothermal conditions. Earth Planet. Sci. Lett. 244, 186–200.

Weaver, J.D., Nguyen, P.D., Parker, M.A., van Batenburg, D., 2005. Sustaining Fracture Conductivity. Society of Petroleum Engineering, SPE, p. 94666.

Weyl, P.K., 1959. Pressure solution and force of crystallization — a phenomenological theory. J. Geophys. Res. 64, 2,001–2,025.